J. Fluid Mech. (1986), *vol.* 173, *pp.* 683–707
Printed in Great Britain

Eulerian and Lagrangian aspects of surface waves

By M. S. LONGUET-HIGGINS

Department of Applied Mathematics and Theoretical Physics, Silver Street, Cambridge CB3 9EW, UK *and* Institute of Oceanographic Sciences, Wormley, Surrey GU8 5UB, UK

(Received 2 May 1986)

Surface waves can be recorded in two kinds of ways, either with a fixed (Eulerian) probe or with a free-floating (Lagrangian) buoy. In steep waves, the differences between corresponding properties can be very marked.

By a simple physical model and by accurate calculation it is shown that the Lagrangian wave period may differ from the Eulerian wave period by as much as 38%. The Lagrangian mean level is also higher than the Eulerian mean, leading to possible discrepancies in remote sensing of the ocean from satellites.

Surface accelerations are of interest in relation to the incidence of breaking waves, and for interactions between short (gravity or capillary) waves and longer gravity waves. Eulerian accelerations tend to be very non-sinusoidal, with large downwards peaks, sometimes exceeding $-g$ in magnitude, near to sharp wave crests. Lagrangian accelerations are much smoother; for uniform gravity waves they lie between $-0.388g$ and $+0.315g$. These values are verified by laboratory experiments. In wind-generated waves the limits are probably wider.

In progressive gravity waves in deep water the horizontal accelerations generally exceed the vertical accelerations. In steep waves, the subsurface accelerations can slightly exceed those at the free surface.

A novel application is made to the rolling motion of ships. In very steep, irrotational waves it is shown theoretically that the flow near the wave crest can lead to the rotation of the hull through angles up to 120° by a single wave, even if the wave is not breaking. This is confirmed by simple experiments. The efficiency of the keel appears to promote capsizing.

1. Introduction

A basic problem in fluid dynamics, to which G. I. Taylor made at least one notable contribution (1921), is the relationship between the Eulerian and the Lagrangian representations of the fluid motion. For sea waves, the two different representations are exemplified by two different types of observation. In the first, measurements of surface elevation are made at a fixed location in the horizontal plane, for example, with a vertical wire gauge or light beam. This type we may call Eulerian. In the second, an accelerometer is mounted vertically in a free-floating buoy which follows more or less the orbital motion of the surface particles. After two time integrations, this gives a Lagrangian measurement of the surface elevation.

For low waves, and to a first approximation in the surface slope, the two types of observation give nearly the same answer; the records obtained have often been assumed equivalent. For steep waves, however, the results can be quite different, as we shall show.

The first effect, discussed in §2 below, concerns the apparent period of the waves.

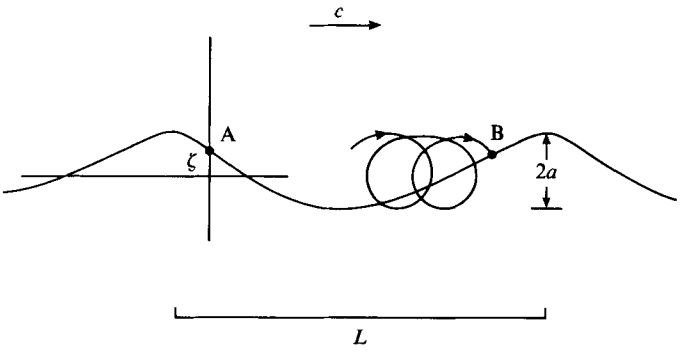

FIGURE 1. Measurement of surface waves with a fixed staff A, and with a free-floating buoy B.

We use a simple model of a limiting wave to demonstrate that, in deep water, the two types of wave motion may differ by as much as 38 %, even in non-breaking waves. The second effect, discussed in §3, is the mean surface level itself. It will be shown that the mean level determined by Lagrangian methods is actually higher than that determined by Eulerian methods, so that significant corrections to some types of remote-sensing observations may have to be made.

A third and important example is that of the vertical accelerations, which are essential to calculating the behaviour of short, centimetric waves riding on the surface of longer gravity waves. This question is discussed in §4.

Lastly we show how the rolling motion of ships may be related to the Lagrangian aspect of the flow in steep, irrotational waves. The problem of the orbital, or Lagrangian, time for the Stokes 120° corner flow is solved analytically, and a numerical computation for the 'almost-highest wave' is calculated. From these solutions it appears that the passage of a single steep wave may cause a ship's hull to roll by angles exceeding 90°. The conclusion is supported by model tests with cylindrical hulls in a laboratory wave channel (§8). The results have clear implications for the capsizing of sailing boats, especially those with efficient keels.

2. The wave period

Consider the period T of a uniform train of waves of wavelength L advancing with speed c, as in figure 1. As measured at a fixed vertical line x = constant, the apparent period is the Eulerian wave period

$$T_{\mathrm{E}} = L/c. \tag{2.1}$$

However, when measurements are made with a floating buoy, we must take into account the mean horizontal velocity, or 'Stokes drift', associated with an irrotational wave. Let U denote the drift velocity at the free surface. Then the wave period as measured by the floating buoy is the Lagrangian period

$$T_{\mathrm{L}} = L/(c-U), \tag{2.2}$$

the difference between (2.1) and (2.2) being due to a Doppler shift. The proportional difference between (2.1) and (2.2) is

$$\frac{T_{\mathrm{L}}-T_{\mathrm{E}}}{T_{\mathrm{E}}} = \frac{U/c}{1-U/c}. \tag{2.3}$$

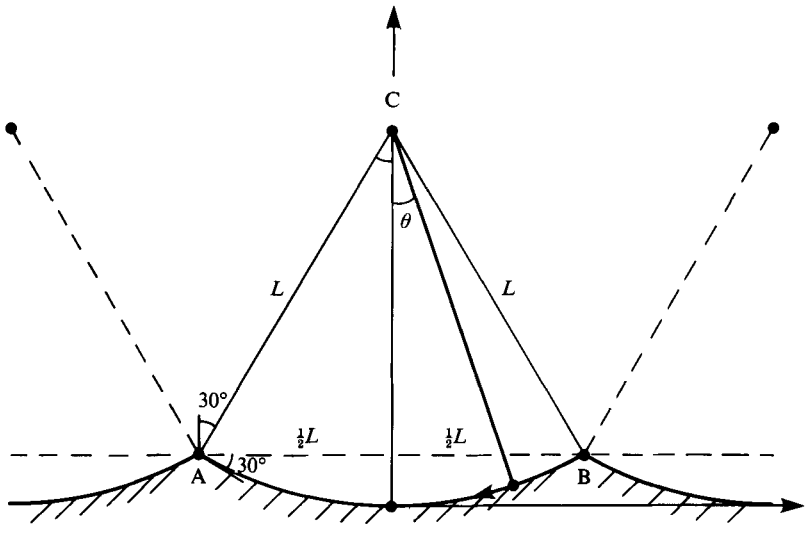

FIGURE 2. The pendulum model of a limiting wave in deep water.

How big is this difference? For low waves, as is well known (Lamb 1932, chap. 9), we have

$$\frac{U}{c} \doteqdot \tfrac{1}{2}(ak)^2, \tag{2.4}$$

where $2a$ denotes the crest-to-trough wave height (figure 1) and $k = 2\pi/L$ is the wavenumber. This is a second-order quantity. On the other hand, in waves of limiting steepness we may estimate U/c using a very simple model (Longuet-Higgins 1979*a*) in which the profile of a deep-water wave of limiting height is approximated by the arc of a circle; see figure 2. Because the tangent to the surface near a crest makes an angle of $\pm 30°$ with the horizontal, the total arc is 60° and the triangle ABC in figure 2 is equilateral. Hence the radius AC of the circle is equal to the wavelength AB, that is L. Further, the pressure gradient being normal to the free surface, the motion of a particle in the surface is the same as that of the bob of a pendulum suspended at the centre C of the circle. This swings from crest B to crest A, then transfers to another pendulum beyond A, and so on. The total motion of a surface particle is the sum of this backward swing together with the forwards phase speed c of the waves. The resulting trajectory, which can be found in terms of an elliptic integral, is shown in figure 3 (curve (1)). This is compared with the trajectory (2) calculated numerically (Longuet-Higgins 1979*b*).

A simple experiment to verify the theoretical trajectory was carried out as follows. In a laboratory wave channel, of width 60 cm and total length 40 m, containing water of mean depth 35 cm, a small wooden bead, painted white, was floated on the water surface at a distance of about 20 m from the wavemaker. This was viewed through a window in the side of the tank. A transient steep wave was generated at the point of observation by building up a spectrum at that point by the method shown in figure 4. The wavemaker generates first the high frequencies, with low group velocities. This is followed by waves of successively lower frequencies, with higher group velocities. A time exposure of the bead's path was taken (figure 5). This shows the beam at first nearly stationary. Then, as the waves arrive, the trajectory uncoils

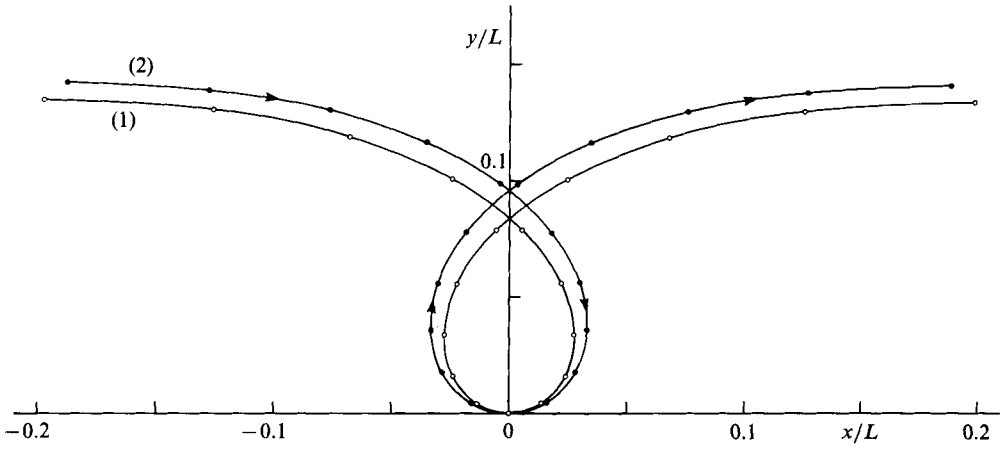

FIGURE 3. Trajectory of a particle in the free surface of a limiting deep-water wave: (1) pendulum approximation, (2) exact calculation.

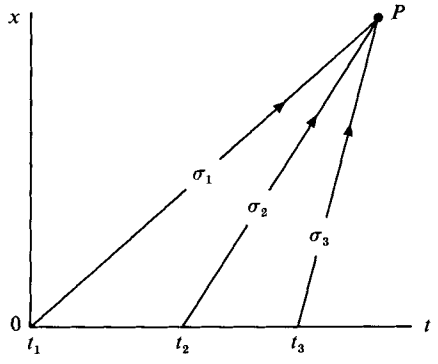

FIGURE 4. The technique for building up a wave spectrum at a distance x and time t from the wavemaker.

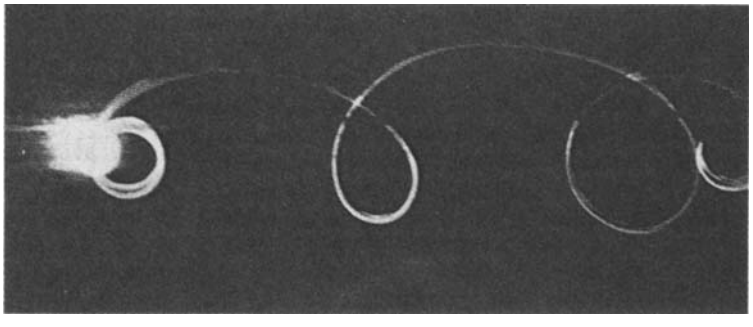

FIGURE 5. Time exposure of a floating bead near the arrival of a wavefront.

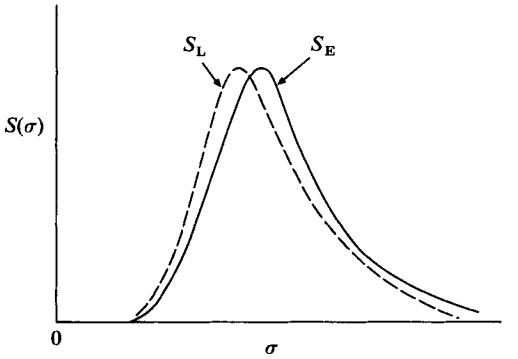

FIGURE 6. Sketch of the frequency spectra of wind waves measured simultaneously by Eulerian and Lagrangian methods.

like a watch-spring. As the steep wave passes the fully developed trajectory is seen. After passage of the steep wave the bead becomes stationary once more.

According to the pendulum model (figure 3) the mean speed of advance of a surface particle is given by $U/c = 0.282$; the accurate value is $U/c = 0.274$, a discrepancy of less than 3%. Now substituting the accurate value into (2.3) we find

$$\frac{T_L - T_E}{T_E} = 0.38, \tag{2.5}$$

a very considerable difference.

In a 'spilling' breaker, if the accelerometer buoy were carried along with the wave like a surf rider, the ratio U/c could become indefinitely large. In practice, accelerometer buoys are usually tethered. Then in a random sea, with groups of high waves separated by relatively low waves, the buoy will tend to be carried forward most by the high waves, and dragged backwards by the mooring during the intervals of lower waves. The resulting frequency spectrum, which is most influenced by the high waves, will still have a significant shift towards lower frequencies, compared to the Eulerian spectrum (see figure 6), but depending on the characteristics of the mooring.

3. The mean surface level

Consider the mean elevation of a marked particle in the free surface. A very general relation, correct to second order, can be proved for fluid particles undergoing small, periodic motions in an inviscid, incompressible and irrotational flow, namely

$$\zeta_L = \zeta_E + \frac{\partial}{\partial z}\tfrac{1}{2}(\Delta \boldsymbol{r})^2, \tag{3.1}$$

where ζ_L and ζ_E are the vertical coordinates of the particle and of the free surface, in Lagrangian and Eulerian coordinates, and

$$\Delta \boldsymbol{r} = \int (u, v)\, \mathrm{d}t \tag{3.2}$$

is the first-order, horizontal displacement of the fluid, in either system (see Srokosz & Longuet-Higgins 1986). A short proof is as follows. To second order,

$$\zeta_L = \zeta_E + \left(\Delta x \frac{\partial \zeta}{\partial x} + \Delta y \frac{\partial \zeta}{\partial y}\right). \tag{3.3}$$

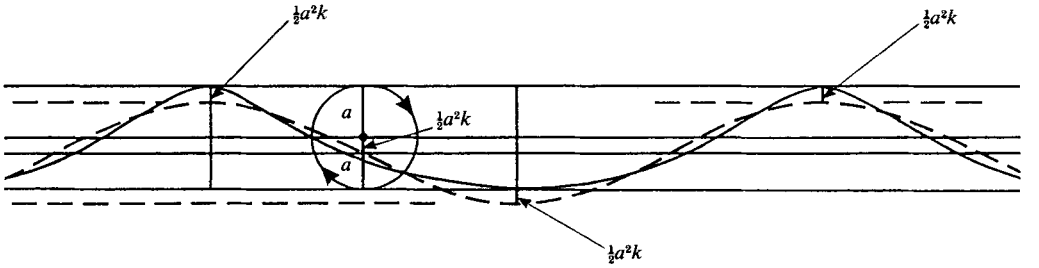

FIGURE 7. Physical interpretation of the difference in mean level as measured by Eulerian and Lagrangian methods.

But

$$\frac{\partial\zeta}{\partial x} = \frac{\partial}{\partial x}\int w\,\mathrm{d}t = \int\frac{\partial w}{\partial x}\,\mathrm{d}t = \int\frac{\partial u}{\partial z}\,\mathrm{d}t = \frac{\partial}{\partial z}\Delta x \tag{3.4}$$

and similarly for $\partial\zeta/\partial y$. On substituting in (3.3) we obtain (3.1).

This can be related to an earlier result (Longuet-Higgins 1953, section 3). For differentiation of (3.1) with respect to t gives

$$w_{\mathrm{L}} = w_{\mathrm{E}} + \frac{\partial}{\partial z}\Big[\int(u, v)\,\mathrm{d}t\cdot(u, v)\Big] \tag{3.5}$$

In the two-dimensional case when $v = 0$ and $(u, w) = (\psi_z, -\psi_x)$ this yields

$$\bar{w}_{\mathrm{L}} = -\frac{\partial}{\partial x}\Big[\bar{\psi}_{\mathrm{E}} + \int\psi_z\,\mathrm{d}t\,\psi_x\Big] = -\Psi_x, \tag{3.6}$$

say, where the overbar denotes the time-average, and similarly $\bar{u}_{\mathrm{L}} = \Psi_y$. In other words Ψ is a stream function for the mass transport (which is therefore non-divergent).

When applied to deep-water waves of amplitude a and wavenumber k, (3.1) yields immediately

$$\bar{\zeta}_{\mathrm{L}} = \bar{\zeta}_{\mathrm{E}} + \tfrac{1}{2}a^2k, \tag{3.7}$$

indicating that the Lagrangian-mean surface level is higher than the Eulerian-mean level by an amount $\frac{1}{2}a^2k$.

A physical interpretation is as follows (see figure 7). Correct to second order, the orbital motion in a deep-water wave is circular, as in a Gerstner wave, but with the added horizontal Stokes drift. The angular velocity of particles in the orbit is uniform, so that the mean height of the particles is that of the centre of the circle. But the upper and lower points of the circle are at the level of the wave crest and the wave trough respectively. Because of the second harmonic in the wave profile, which makes the crests sharper and the troughs flatter, the crest and trough are both raised, relative to the first harmonic, by an amount just equal to the amplitude of the second harmonic. But this is $\frac{1}{2}a^2k$ (see Lamb 1932, chap. 9). Hence the centre of the circular orbit is raised by the same amount.

The formula (3.1) is very general and can be applied to waves with a continuous spectrum (see below) and also to subsurface motions. But it is correct only to second order. We now prove a very simple relation for uniform, progressive, irrotational waves which is *exact* up to all orders of magnitude, namely

$$\bar{\zeta}_{\mathrm{L}} - \bar{\zeta}_{\mathrm{E}} = \frac{cU}{2g}, \tag{3.8}$$

U being the horizontal drift velocity at the free surface.

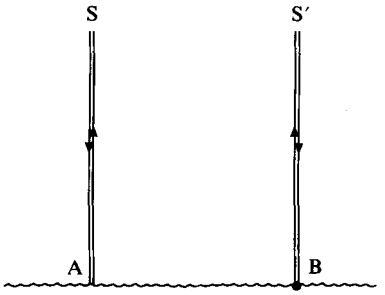

FIGURE 8. Observation of mean level by transmission between a satellite S and the sea surface.

Take axes moving with the phase-speed c, and for convenience choose the origin of z at a level such that in Bernoulli's equation

$$\frac{p}{\rho}+\tfrac{1}{2}q^2+gz = \text{constant} \tag{3.9}$$

the right-hand side is zero. Then at the free surface, where p vanishes, we have

$$\tfrac{1}{2}q^2+g\zeta = 0, \tag{3.10}$$

while at great depths, where $q\to c$, we have

$$\frac{p}{\rho}+\tfrac{1}{2}c^2+gz\to 0. \tag{3.11}$$

Now since at great depths $w\to 0$, there is in the limit no vertical flux of momentum across the horizontal plane $z =$ constant. So by considering the vertical momentum between this plane and the free surface $z = \zeta$ we obtain

$$\frac{p}{\rho}+g(z-\bar{\zeta}_{\mathrm{E}})\to 0 \tag{3.12}$$

(cf. Lamb 1932, p. 420). From the last two equations it follows that

$$\bar{\zeta}_{\mathrm{E}} = -\frac{c^2}{2g}. \tag{3.13}$$

Consider now the Lagrangian-mean level ζ_{L}. In general, the orbital time t satisfies

$$\mathrm{d}t = \frac{\mathrm{d}\phi}{q^2}, \tag{3.14}$$

where q is the velocity potential in the moving reference frame. So for the mean level we have

$$\bar{\zeta}_{\mathrm{L}} = \frac{1}{T_{\mathrm{L}}}\int\zeta\,\mathrm{d}t = \frac{1}{T_{\mathrm{L}}}\int\frac{\zeta}{q^2}\,\mathrm{d}\phi. \tag{3.15}$$

Then using (3.10) we obtain

$$\bar{\zeta}_{\mathrm{L}} = \frac{1}{2gT_{\mathrm{L}}}\int\mathrm{d}\phi = \frac{-cL}{2gT_{\mathrm{L}}} = \frac{-c^2}{2g}\frac{T_{\mathrm{E}}}{T_{\mathrm{L}}}. \tag{3.16}$$

From (3.13) and (3.16) it follows that

$$\bar{\zeta}_{\mathrm{L}}-\bar{\zeta}_{\mathrm{E}} = \frac{c^2}{2g}\left(1-\frac{T_{\mathrm{E}}}{T_{\mathrm{L}}}\right) = \frac{c^2}{2g}\frac{U}{c} \tag{3.17}$$

by (2.1) and (2.2). This proves the result.

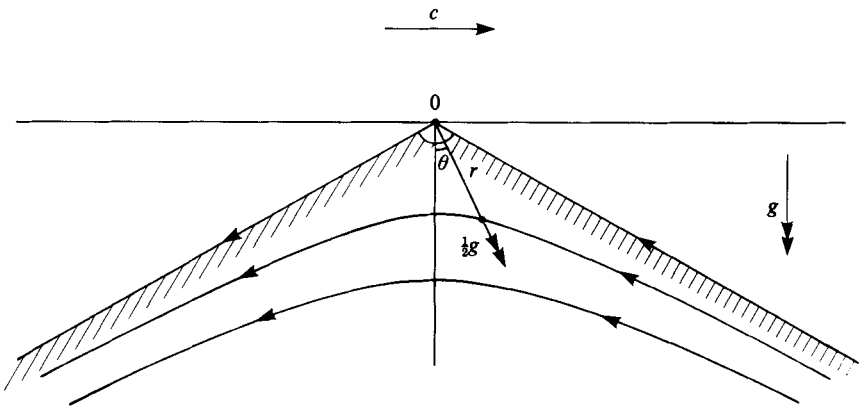

FIGURE 9. Streamlines and particle accelerations in a Stokes 120° corner flow.

In particular, for limiting waves, when $c^2 = 1.1931\,g/k$ and $U/c = 0.274$ (see §2) we have

$$\bar{\zeta}_{\mathrm{L}} - \bar{\zeta}_{\mathrm{E}} = 0.0260L. \tag{3.18}$$

Such differences may have practical implications for the observation of mean sea level from satellites. Suppose, for instance, that a signal is transmitted from a floating buoy B to an overhead satellite and back, as in figure 8. The total elapsed time is a measure of the vertical separation between them. But a different answer will be obtained if, instead, a transmitter is placed in the satellite and the time is measured for reflection back off the sea surface at A. This difference is, by (3.7), of order $\overline{(ak)^2}L/4\pi$, where L is the dominant wavelength and a bar denotes the average. For a wind-generated wavefield $\overline{(ak)^2}$ may be as high as 0.012, indicating that the difference in mean level is of the order of 1 % of the dominant wavelength. For waves of period say 6 s this amounts to about 0.5 m. Such a figure is easily detectable by modern instruments, and is significant for the estimation of geostrophic currents.

In some applications of remote sensing it is useful to know the moments of the distribution of the sea-surface elevation, particularly the third moment, giving the coefficient of skewness. The general relation (3.1) can be used to obtain such parameters in terms of the two-dimensional spectrum of the surface (see Srokosz & Longuet-Higgins 1986).

4. Vertical accelerations

The surface accelerations in a field of wind-generated waves are of particular interest for many reasons. First because of their relation to wave breaking. Phillips (1958) argued that if the free surface were to develop a sharp crest, then the downwards acceleration at that point should be equal to $-g$, as shown experimentally by Taylor (1953) in a standing wave of limiting amplitude. However, it turns out that in a *progressive* wave of limiting amplitude, where the flow near the crest is similar to the Stokes 120° corner flow (figure 9) the vector acceleration is everywhere $\frac{1}{2}g$ directed away from the crest (Longuet-Higgins 1963). In an almost-highest wave, the downwards acceleration at the crest is only $0.388g$ (Longuet-Higgins & Fox 1977; Williams 1985). Experimentally, Ochi & Tsai (1983) found that irregular progressive waves break at a steepness rather less than that of the limiting steady wave, and a limiting value $0.40g$ has been suggested by Srokosz (1986).

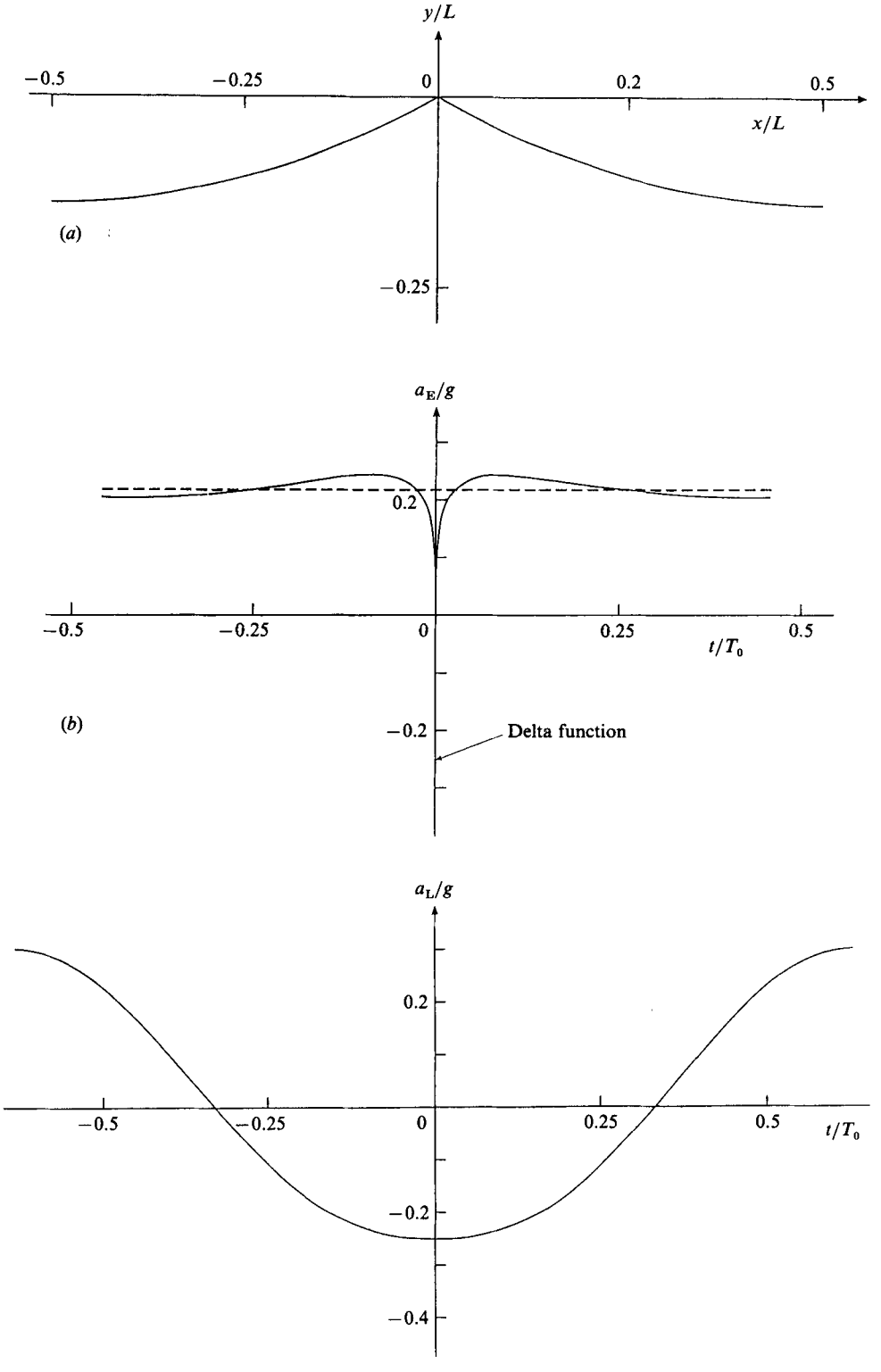

FIGURE 10. (*a*) Exact profile of a limiting gravity wave on deep water ($ak = 0.4432$). (*b*) The apparent (Eulerian) vertical acceleration corresponding to (*a*). (*c*) The real (Lagrangian) vertical acceleration corresponding to (*a*) (plotted against the orbital time).

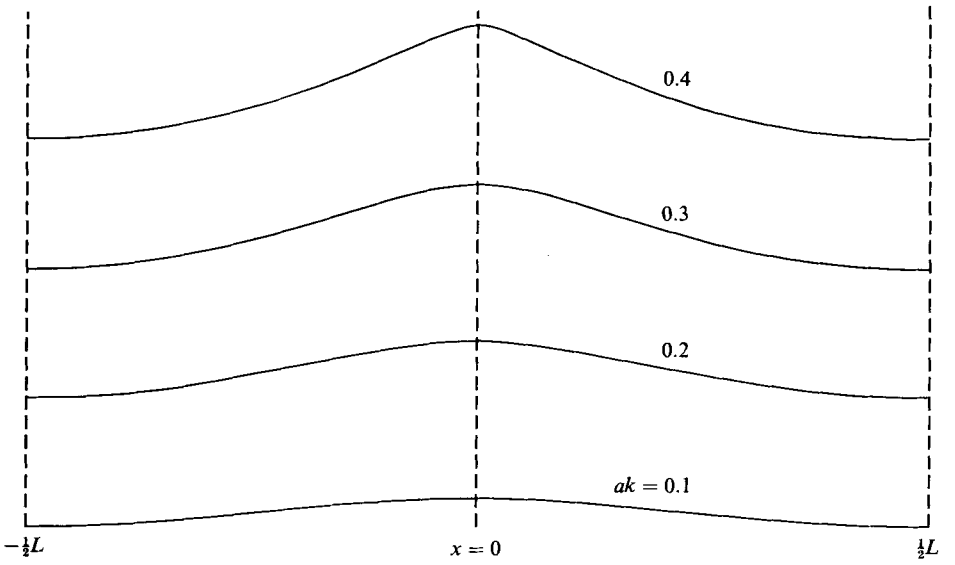

FIGURE 11. Surface profiles of gravity waves in deep water, at steepnesses $ak = 0.1$, 0.2, 0.3 and 0.4.

In discussing the problem it is clearly necessary to distinguish between Eulerian and Lagrangian accelerations. In Eulerian measurements, if the surface elevation at a fixed vertical line is denoted by $\zeta(t)$, then in a progressive wave the apparent vertical velocity is $\zeta_t = -c^{-1}\zeta_x$, where c is the phase speed. Similarly the apparent vertical acceleration is

$$a_{\mathrm{E}} = \zeta_{tt} = c^{-2}\zeta_{xx}, \tag{4.1}$$

showing that the acceleration is closely related to the *curvature* of the free surface. For a limiting wave on deep water, this acceleration is shown in figure 10(*b*). Over nearly all the wave, the surface profile (figure 10*a*) is concave upwards, and so the acceleration is positive, with almost constant value $0.22g$. Near the crest, where the curvature is sharply negative, the acceleration is negatively infinite; there is a delta function of such a magnitude as to make the total mean vertical acceleration, integrated over one wave period, vanish precisely. The resulting curve is hardly sinusoidal.

The Lagrangian acceleration, on the other hand, is shown in figure 10(*c*). This can be found from the general relation

$$\boldsymbol{a}_{\mathrm{L}} = \boldsymbol{u}\cdot\nabla\boldsymbol{u} \tag{4.2}$$

where $\boldsymbol{u}$ is the steady fluid velocity in a frame of reference travelling with the phase speed. Alternatively we may note that the components of the acceleration tangential and normal to the free surface are given by

$$a_{\mathrm{s}} = -g\sin\beta, \quad a_{\mathrm{n}} = \frac{q^2}{R}, \tag{4.3}$$

where β is the angle between the tangent and the horizontal, q is the local particle speed (in the moving frame of reference) and R is the radius of curvature of the surface. To get the vertical component a_{L} of the real (Lagrangian) acceleration we resolve both these components in the upwards direction. Near (but not at) the wave crest, q is small, R is finite and β is 30°, showing that a_{L} equals $-\frac{1}{4}g$. In the wave

trough, on the other hand, $\sin\beta$ vanishes and $q^2 = 2gH$, where H is the wave height. The pendulum model (§2) suggests that $H \doteqdot (1-3^{\frac{1}{2}}/2)\,L$, while $R = L$, giving

$$a_{\mathrm{L}} = (2-3^{\frac{1}{2}})\,g = 0.268g, \tag{4.4}$$

almost equal and opposite to the crest acceleration. From figure 10(*c*) it can be seen that the Lagrangian acceleration is in fact almost sinusoidal in time.

The particle accelerations in deep-water gravity waves of arbitrary amplitude have been calculated accurately in a recent paper by the author (Longuet-Higgins 1985). Surface profiles in the cases $ak = 0.1$, 0.2, 0.3 and 0.4 are shown in figure 11. The corresponding apparent (Eulerian) accelerations are shown in figure 12, from which it is clear that even in the case $ak = 0.2$ the accelerations are markedly non-sinusoidal. When $ak = 0.4$ (i.e. 10% less than the maximum 0.4432) the apparent acceleration at the crest is already $-1.8\,g$, so that a floating bead constrained to slide on a thin, frictionless wire would presumably leave the free surface altogether.

The real (Lagrangian) accelerations are shown in figure 13. These are much more sinusoidal, except that for near-limiting waves there is a singularity, described by the theory of the almost-highest wave (Longuet-Higgins & Fox 1977, 1978). Figure 14 shows the asymptotic form of the free surface, plotted on a lengthscale

$$l = q^2/2g, \tag{4.5}$$

where q is the particle speed at the wave crest relative to an observer moving with the phase speed c. If we define a small parameter ϵ by

$$\epsilon^2 = q^2/2c_0^2, \tag{4.6}$$

where $c_0 = (g/k)^{\frac{1}{2}}$ is the linear phase speed of the wave, then clearly $\epsilon^2 = kl$. It can also be shown that for deep-water waves

$$\epsilon^2 \doteqdot 2.0\,|ak-(ak)_{\max}| \tag{4.7}$$

(see Longuet-Higgins & Fox 1978).

The crosses in figure 14 indicate the precisely calculated surface profile; the circular plots indicate an analytic approximation given by

$$z = \frac{\alpha - \mathrm{i}\gamma\chi}{(\beta-\mathrm{i}\chi)^{\frac{1}{3}}}, \tag{4.8}$$

where $\chi = \phi + \mathrm{i}\psi$ is the (complex) velocity potential and α, β, γ are suitably chosen constants (see Longuet-Higgins 1979*c*). The two curves agree closely. However, the analytic approximation is more convenient for calculating the Lagrangian accelerations, through (4.2). In figure 15 these are shown plotted against the scaled time t/ϵ. One can see the transition from the values $-0.25g$ on each side of the wave crest to the value $-0.388g$ at the crest itself.

The *horizontal* component of the Lagrangian acceleration can be appreciable, as is seen by considering that a particle at the crest of a limiting wave travels with the phase speed c; the same particle has been accelerated to this forward speed from a negative speed in the preceding wave trough, in a little over half a wave period T. The acceleration is therefore of order $2c/T$, or g/π on linear theory. The accurately calculated horizontal accelerations are shown in figure 16. It can be seen that in magnitude these actually exceed the vertical accelerations. This implies that a sailor in a small boat will be tossed to and fro horizontally as much as vertically.

The subsurface accelerations are also surprising. From the fact that in the almost-highest wave (figure 14) the crest acceleration is less than the acceleration at

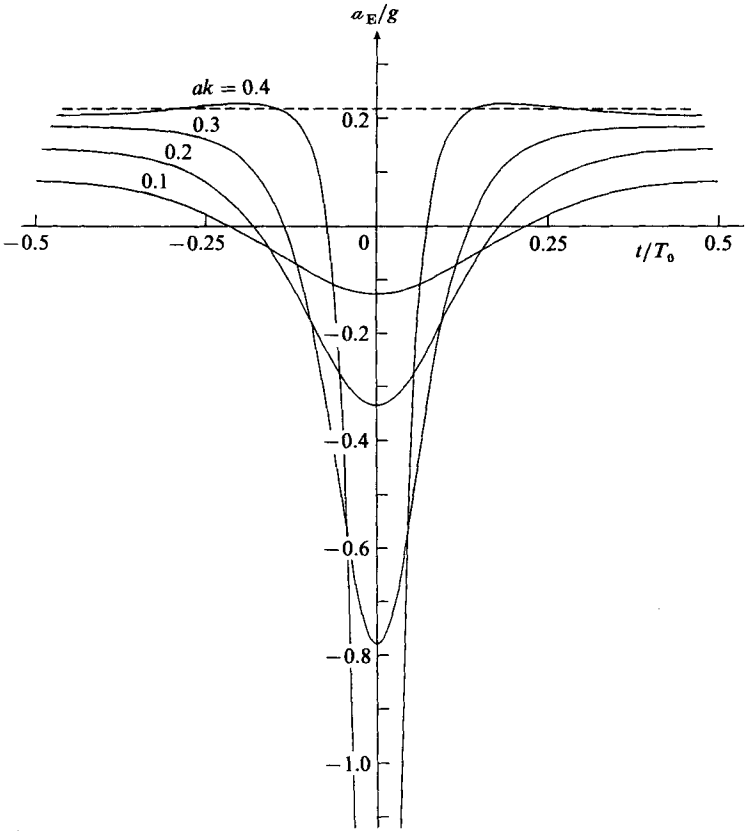

FIGURE 12. The apparent (Eulerian) accelerations of the free surface in gravity waves of steepnesses $ak = 0.1$, 0.2, 0.3 and 0.4.

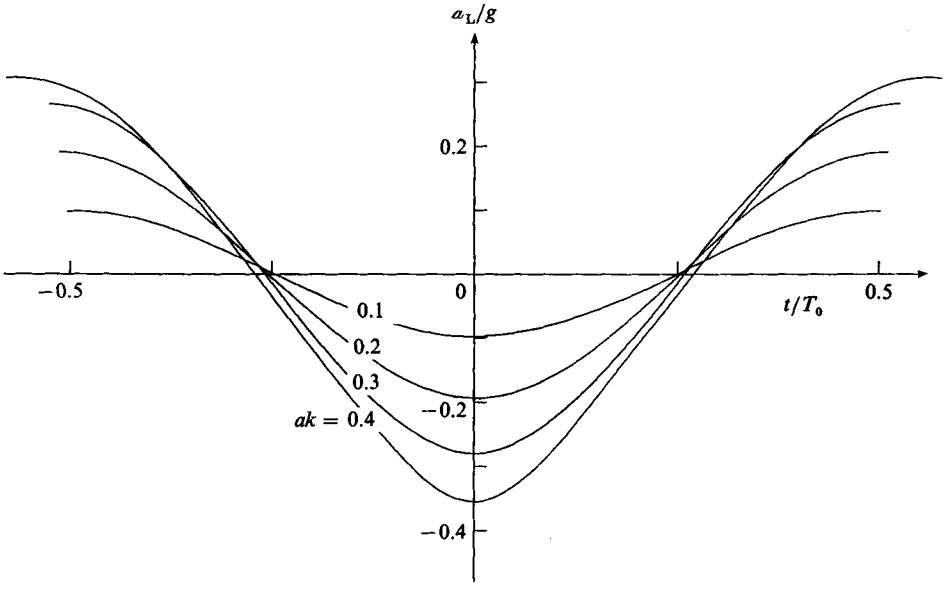

FIGURE 13. The real (Lagrangian) vertical accelerations at the free surface in gravity waves of steepnesses $ak = 0.1$, 0.2, 0.3 and 0.4.

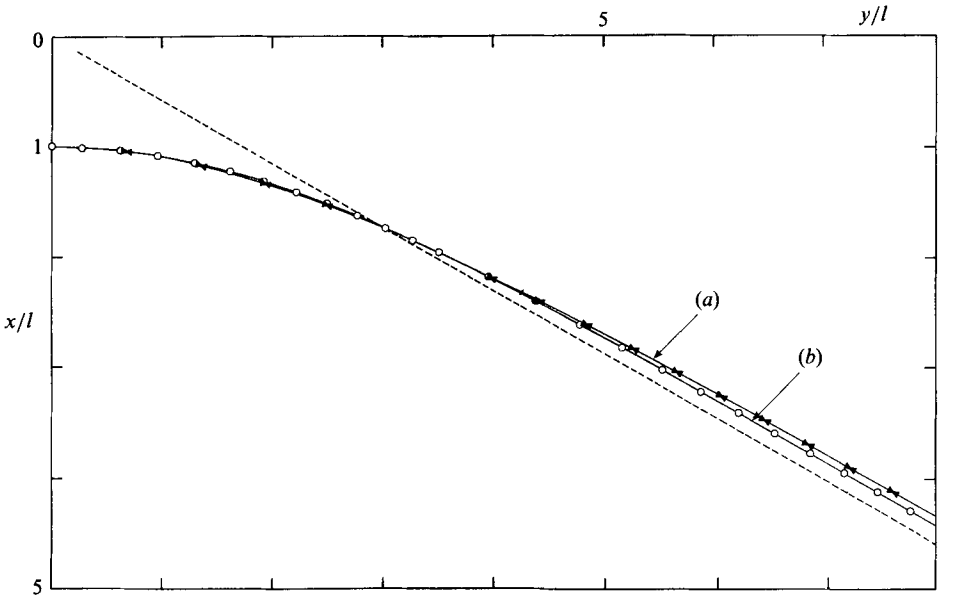

FIGURE 14. Surface profile of the crest of an almost-highest wave: (*a*) exact calculation; (*b*) approximate analytic expression.

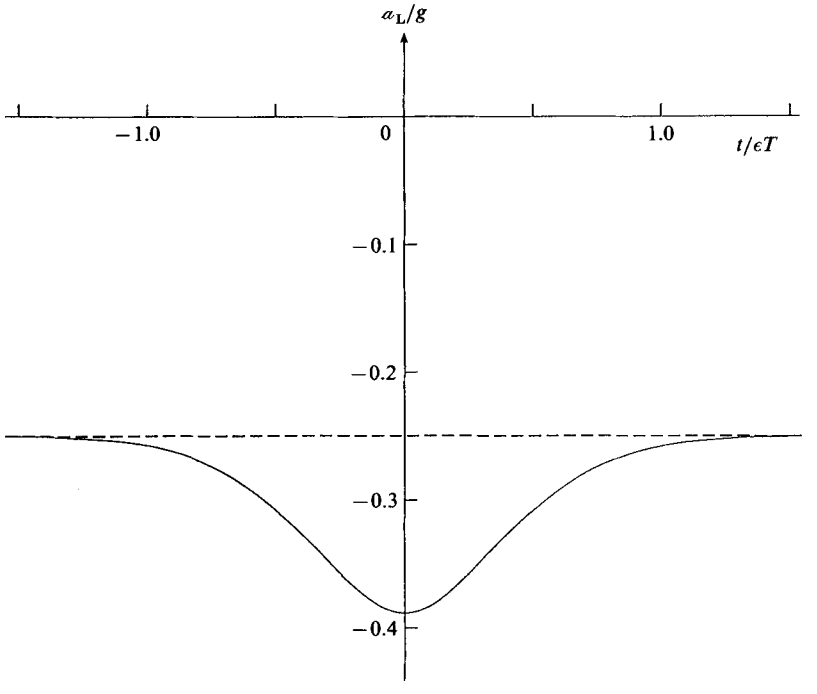

FIGURE 15. Vertical component of the real (Lagrangian) acceleration in an almost-highest wave, plotted against the scaled time t/ϵ.

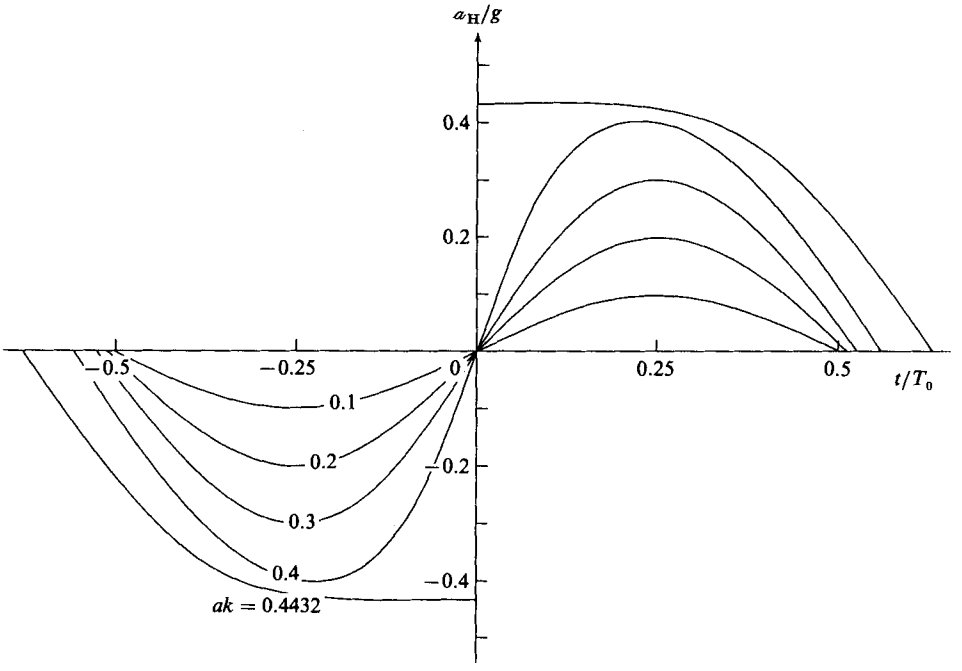

FIGURE 16. Horizontal component of the real (Lagrangian) acceleration at the surface of deep-water waves of steepnesses $ak = 0.1$, 0.2, 0.3, 0.4 and 0.4432.

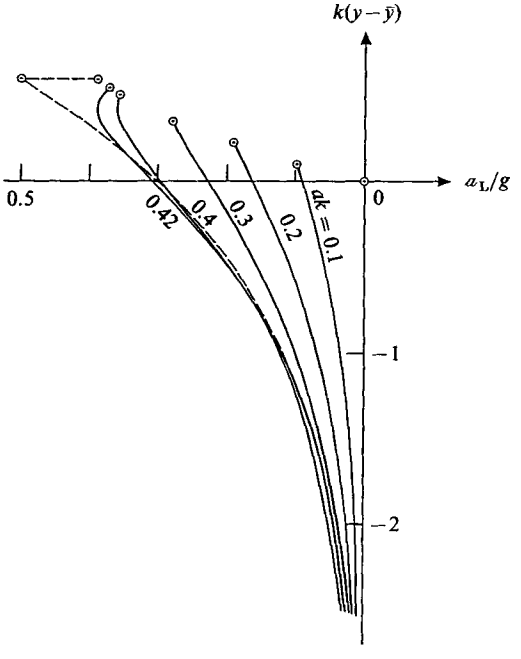

GURE 17. Subsurface accelerations: vertical component of the Lagrangian acceleration vertically eneath the crest of gravity waves, when $ak = 0.1$, 0.2, 0.3, 0.40, 0.42 and 0.4432 (broken line).

infinity ($\frac{1}{2}g$), one may infer that in very steep waves the vertical acceleration beneath the crest must actually *increase* with depth, at first. This is confirmed by the accurate calculations shown in figure 17.

One further reason for our interest in surface accelerations is the important application to remote sensing of the sea surface. Most of the reflection of electromagnetic radiation from X or L-band radars is due to Bragg scattering by gravity or capillary waves of lengths 20 cm or less. The question of how such short waves interact with longer gravity waves is thus important for understanding the radar imaging of the sea surface. The propagation of the short waves is, however, controlled by the effective gravity, hence the orbital accelerations, in the longer waves. Already it can be seen from figure 13 that for long waves of steepness $ak = 0.40$, for example, the effective gravity varies from $0.65g$ at the wave crest to $1.30g$ in the trough. The results of such nonlinearities for the propagation of the short waves have been evaluated (Longuet-Higgins 1986), and found to produce changes in the short-wave steepness by a factor of 10 or more. This is to be compared with a factor less than 2 given by linear theory.

5. Experimental verification

To measure the *Lagrangian* accelerations, experiments were conducted in the wave channel at IOS, Wormley, which is 60 m long, 2 m wide and 2.7 m deep. Waves of period 1.20–1.40 s were generated by the wedge-shaped plunger at one end ($x = 0$) in water of mean depth 1.78 m. The waves were observed at a distance $x = 36$ m from the wavemaker, with a small piezo-electric accelerometer contained, together with amplifier and power supply, in a flat cylindrical container of diameter 9.6 cm and thickness 3.2 cm (see figure 18). The output was brought by thin leads to a standard recording millivoltmeter. Calibration was carried out by simply inverting the accelerometer so as to measure the difference between $-g$ and g. The voltage output was linear up to $3g$.

The accelerometer was fixed rigidly in relation to the float and so tended to respond to the component of the acceleration normal to the free surface, not the vertical component, in general. Hence, the accelerations were noted only at the wave crests and wave troughs, where the normal and the vertical components coincide.

To avoid 'noise' from the second and higher harmonics produced by the plunger, observations were always made near the front of the wavetrain, which arrived at about the theoretical time $2\sigma x/g$ after starting the wavemaker, as described in Longuet-Higgins (1974). For crest accelerations, the largest wave at the head of the wavefront was chosen. Its height usually exceeds that of the steady wavetrain behind by about 20%. For trough accelerations, the two adjacent wave troughs were selected, the wave period T being taken as the time interval between the two troughs. The wave height $2a$ was observed visually against a flat vertical scale at one side of the tank.

Figure 19 shows the results. The horizontal coordinate is the steepness parameter ak, where $k = (c/c_0)\, k_0$, the suffix referring to the values for linear waves. Thus $k_0 = \sigma^2/g$ where $\sigma = 2\pi/T$. The ratio c/c_0 was taken from the calculated values in table 2 of Longuet-Higgins (1975). The upper and lower curves in figure 19 show the trough and crest accelerations respectively. The theoretical values (circular plots) are taken from table 1 of Longuet-Higgins (1985).

Generally the agreement between theory and observation is good, though there is

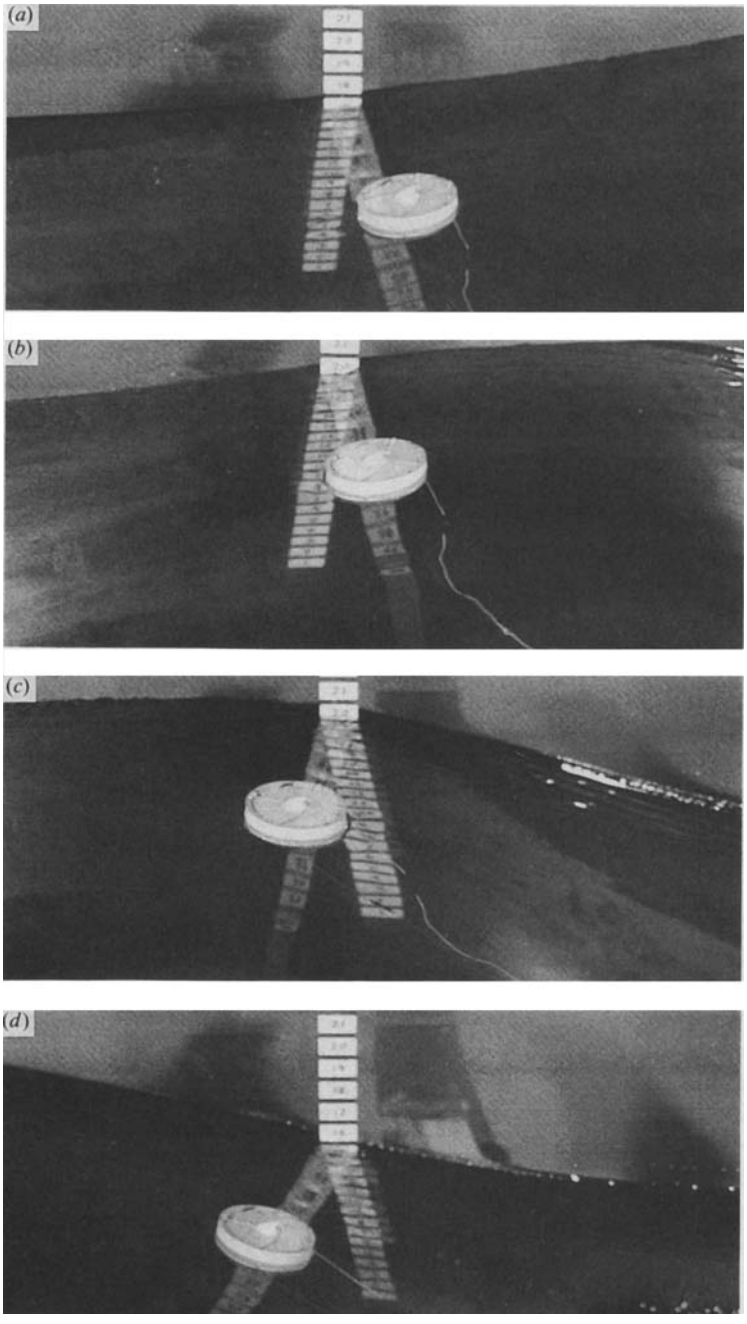

FIGURE 18. The floating accelerometer in position in the 60 m wave tank at IOS, Wormley. The vertical scale is in inches.

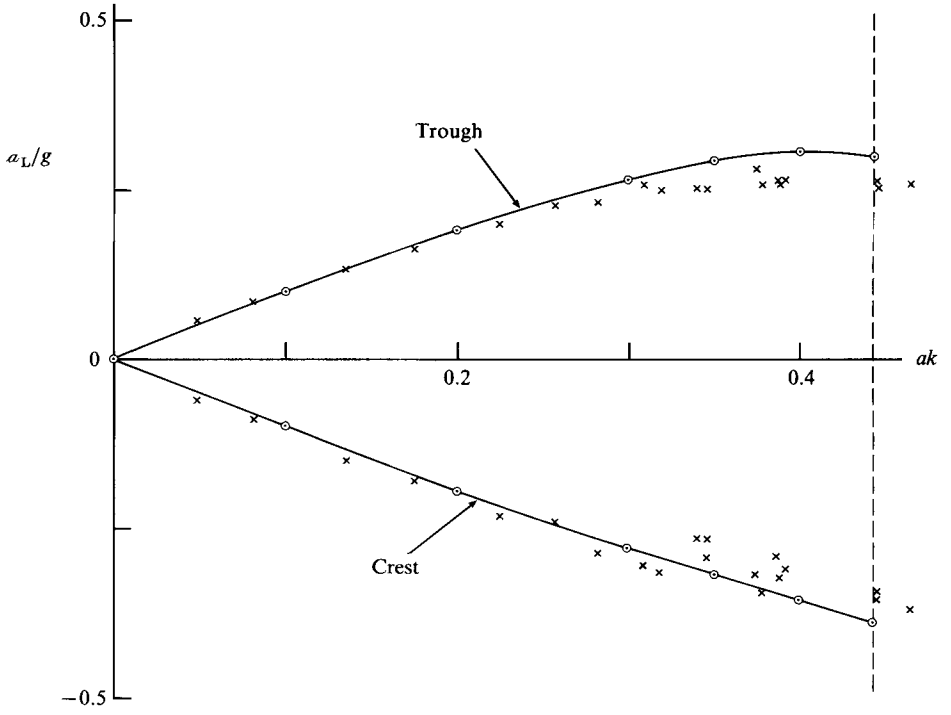

FIGURE 19. Vertical Lagrangian accelerations at the crest and trough of gravity waves, as a function of the wave steepness ak: —⊙—, calculated; ×, observed.

increased scatter at higher wave steepnesses. We note that the radius of curvature R at the crest will become comparable with the diameter d of the float when

$$d \sim R = \frac{5.15\epsilon^2}{k_0}$$

(see Longuet-Higgins & Fox 1977, 1978). Hence

$$|ak-(ak)_{\max}| \sim \frac{kd}{10.2} = 0.025$$

and it is not surprising to find discrepancies when $ak > 0.40$. The dynamic response of the buoy becomes significant only when its natural period $(d/g)^{\frac{1}{2}}$ is comparable to the timescale k/q at the crest. This occurs only when $|ak-(ak)_{\max}| \sim 0.002$.

That the *Eulerian* accelerations can easily exceed $-g$ is verified immediately from the existence of regular waves with a crest curvature exceeding g/c^2, or k approximately. However, the first confirmation of such accelerations in wind-waves was made from field observations in the Queen Elizabeth II reservoir near Staines, Middlesex (see figure 20). The waves were recorded by fixed capacitance-wire gauges at the tower near the south-eastern corner. Winds were usually from the north and west. Table 1, taken from a recent paper by Ewing, Longuet-Higgins & Srokosz (1986), shows the maximum and minimum apparent accelerations in records of 1000 s duration, at different wind speeds. It will be seen that the downwards acceleration on one occasion was as great as $-1.6g$. Further details are given in the paper just mentioned.

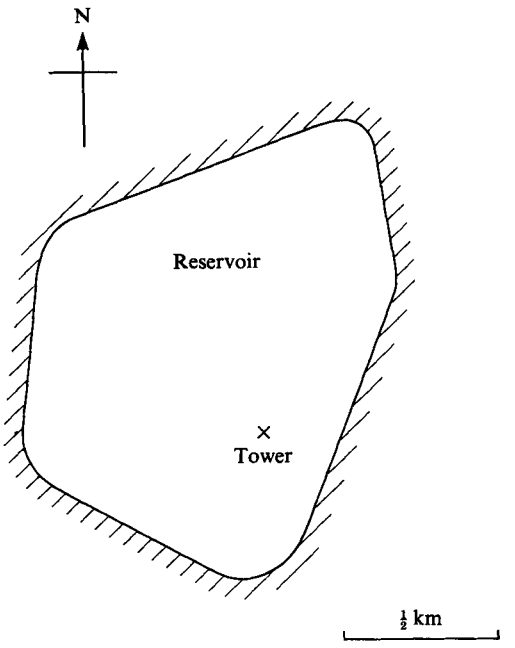

FIGURE 20. Plan of the Q. Elizabeth II reservoir near Staines, Middlesex, showing the site of the Eulerian wave measurement.

Date	Starting time (EMT)	Wind speed (m/s)	Wind direction (deg)	a_E/g min	a_E/g max.
21 Apr. 1982	1308	3.7	050	−1.11	0.78
21 July 1982	1343	7.1	020	−0.97	0.68
22 Mar. 1983	1310	12.4	270	−1.60	0.78
24 Mar. 1983	1229	10.8	000	−1.26	0.73
16 Apr. 1984	1330	7.0	310	−1.13	0.62

TABLE 1. Maximum and minimum Eulerian accelerations in wind waves, measured in the Queen Elizabeth II reservoir

6. Angular motion of floating bodies

The rolling motion of ships is the subject of an extensive literature; for an excellent review see Himeno (1981). Nearly all studies seem to have considered the linear, or the nonlinear, response of the ship's hull to sinusoidal waves. Here we wish to point out that in very steep waves the nonlinearity of the waves themselves is an important, perhaps overriding, factor. The form of the steep gravity-wave crest introduces new length- and timescales. Moreover, the motion of a ship in such steep waves may be more suitably treated from a Lagrangian rather than from a Eulerian point of view.

Consider the rolling motion of a cylindrical body in two-dimensional waves, as in figure 21, where the maximum diameter d of the body is small compared to the wavelength L. We may distinguish two extreme types of rolling motion. The first occurs when the body has strong rolling stability and a relatively short free period

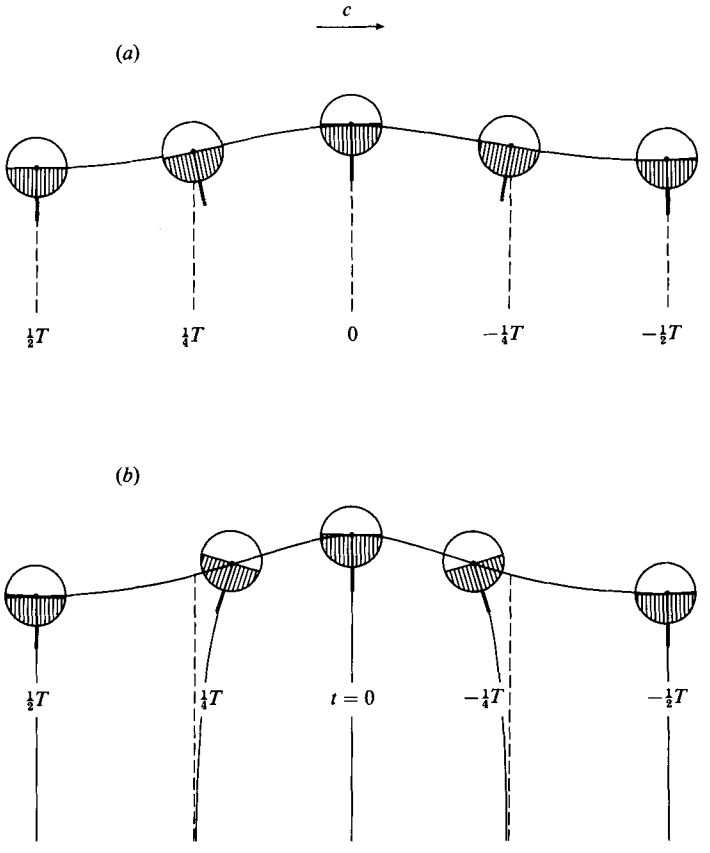

FIGURE 21. Types of rolling motion for a floating cylindrical hull: (*a*) hydrostatic, (*b*) inertial.

of roll. It tends then always to align itself in the direction of effective gravity, which is normal to the free surface (figure 21*a*). We may call this 'hydrostatic rolling'.

The second type occurs when the body has very little roll stability, and inertial or acceleration forces acting on the keel, as well as tangential frictional forces, compel it to respond to velocity gradients in the wave motion (figure 21*b*). We may call this 'inertial rolling', and it is evident that in this case the angular displacements are exactly opposite in sense to those in case (*a*). For on a wave crest, for instance, the orbital motion beneath the surface is backwards relative to the crest. So if the 'keel' follows the particle motion in its vicinity, the body will rotate *clockwise*. In a wave trough, on the other hand, the orbital motion is backwards, and decreases with depth, so the body rotates anticlockwise.

In case (*b*) the orientation of the keel closely follows the position of a nearly vertical line of particles at any given orbital time t. These are indicated in the figure for relatively low waves. (It is assumed that the keel starts in a vertical position in the wave trough.)

As the wave steepness is increased, the hydrostatic forces involved in type (*a*) rolling, which will grow roughly linearly with wave steepness, will tend to be overtaken by the inertial forces in type (*b*) rolling, which are generally nonlinear. Thus for very steep waves, and with an efficient keel, it may happen that type (*b*) rolling is typical.

The question, then, that we wish to investigate, is the determination of the loci of constant orbital time near the crests of steep gravity waves. Essentially this will constitute a Lagrangian description of the wave motion.

7. Orbital times for steep waves

A general formula for the orbital time t of a particle in a steady, irrotational flow with complex potential $\chi = \phi + \mathrm{i}\psi$ is

$$t = \int \frac{\mathrm{d}\phi}{q^2} = \int \left|\frac{\mathrm{d}z}{\mathrm{d}\chi}\right|^2 \mathrm{d}\phi, \tag{7.1}$$

where q is the local particle speed, and the integral is taken along a streamline ψ = constant (see Longuet-Higgins 1979*b*).

Consider first the Stokes corner flow shown in figure 9. For this flow we have

$$\chi = \phi + \mathrm{i}\psi = \tfrac{2}{3}\mathrm{i}g^{\frac{1}{2}} z^{\frac{3}{2}} \quad \text{where } z = x + \mathrm{i}y = r\,\mathrm{e}^{\mathrm{i}\theta} \tag{7.2}$$

in a frame of reference moving with the wave (x being measured vertically downwards). On inversion this gives

$$z = (\tfrac{3}{2})^{\frac{2}{3}}\,\mathrm{e}^{-\mathrm{i}\pi/3} g^{-\frac{1}{3}} \chi^{\frac{2}{3}}, \tag{7.3}$$

and on substituting in (7.1)

$$t = \left(\frac{2}{3g}\right)^{\frac{2}{3}} \int_0^{\phi} \frac{\mathrm{d}\phi}{(\phi^2 + \psi^2)^{\frac{1}{3}}}. \tag{7.4}$$

Hence writing

$$\mu = \frac{\phi}{\psi} = -\tan\tfrac{3}{2}\theta \tag{7.5}$$

we obtain

$$t = \frac{2}{3}\left(\frac{r}{g}\right)^{\frac{1}{2}} \frac{I(\mu)}{(1+\mu^2)^{\frac{1}{6}}}, \tag{7.6}$$

where

$$I(\mu) = \int_0^{\mu} \frac{\mathrm{d}\mu}{(1+\mu^2)^{\frac{1}{3}}}. \tag{7.7}$$

Equation (7.6) expresses the orbital time t as the product of a function of r and a function of θ. It is thus a self-similar solution. Hence it is easy to express r as a function of t and θ, and we find

$$r = \frac{\frac{9}{4}gt^2(1+\mu^2)^{\frac{1}{3}}}{[I(\mu)]^2}, \tag{7.8}$$

the required expression.

The curves of constant t are shown in figure 22. Near the free surface $\theta = \frac{1}{3}\pi$, when $\mu \to \infty$, we have $I(\mu) \sim 3\mu^{\frac{1}{3}}$ and so $r \to \frac{1}{4}gt^2$, as we would expect. Generally from (7.7) we have

$$I(\mu) = 3\mu^{\frac{1}{3}} - A + B(\mu), \tag{7.9}$$

where

$$A = \int_0^{\infty} \left[\frac{1}{\mu^{\frac{2}{3}}} - \frac{1}{(1+\mu^2)^{\frac{1}{3}}}\right] \mathrm{d}\mu = 2.239 \tag{7.10}$$

and

$$B(\mu) = \int_{\mu}^{\infty} \frac{1}{\mu^{\frac{2}{3}}} [1 - (1+\mu^{-2})^{-\frac{1}{3}}]\,\mathrm{d}\mu \sim -\frac{\mu^{-\frac{5}{3}}}{5} \tag{7.11}$$

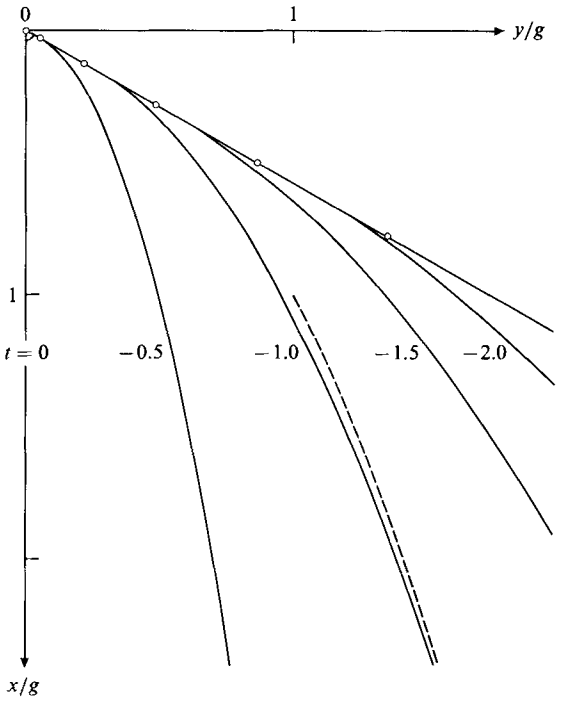

FIGURE 22. Curves of constant orbital time t in a Stokes 120° corner flow.

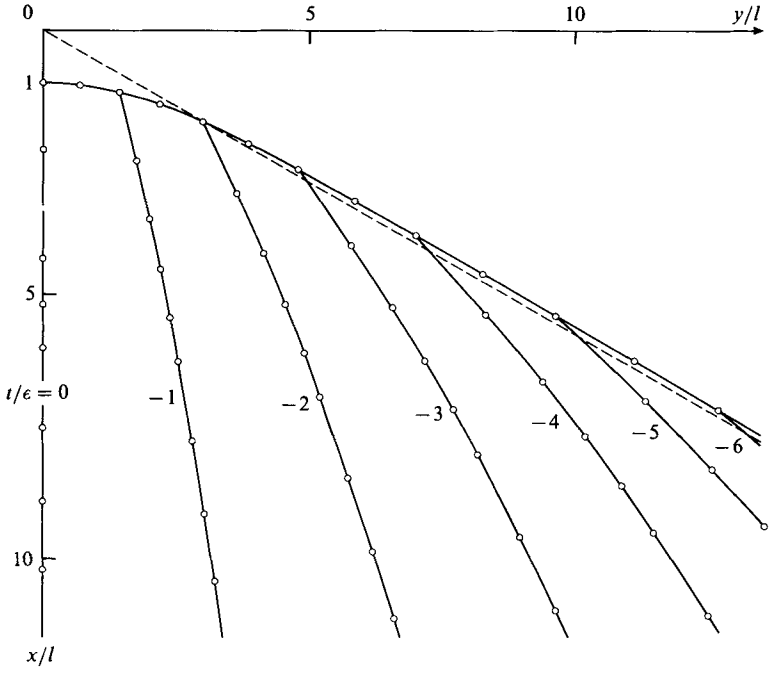

FIGURE 23. Curves of constant orbital time t in an almost-highest wave.

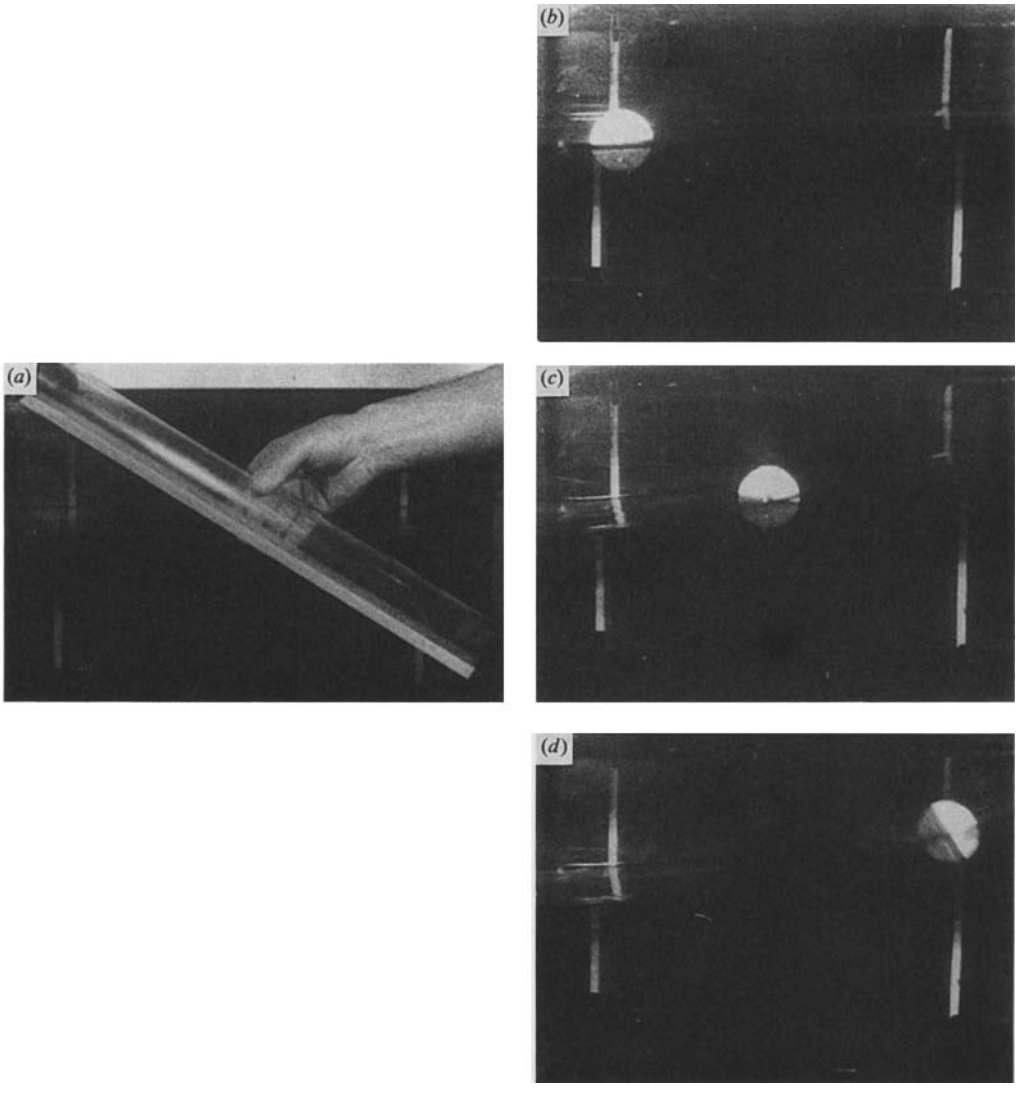

FIGURE 24. (*a*) Cylindrical model, with keel. (*b*) Model in low waves: $ak = 0.07$. (*c*) Model in steeper waves: $ak = 0.23$. (*d*) Model in very steep waves: $ak = 0.39$.

for large μ. Hence when $\theta \to \frac{1}{3}\pi$,

$$r \sim \tfrac{1}{4}gt^2\left[1+\tfrac{2}{3}A\left(\frac{3\theta'}{2}\right)^{\frac{1}{3}}\right], \tag{7.12}$$

where $\theta' = \frac{1}{3}\pi - \theta$. So at the free surface, $\mathrm{d}r/\mathrm{d}\theta$ becomes infinite, and the line of particles with t = constant becomes tangential to the free surface.

As $\theta \to 0$, on the other hand, we see that $y \sim qt$ where q is the particle speed on the line $\theta = 0$. From (7.2) it follows that $y \sim g^{\frac{1}{2}}tx^{\frac{1}{2}}$, a parabola. The asymptote when $t = 1$ is shown by the broken line in figure 22.

Assuming that the keel swings round with the curves of constant t in figure 22, we see that the floating body could in theory be turned through an angle of up to 120° on passage of the wave crest.

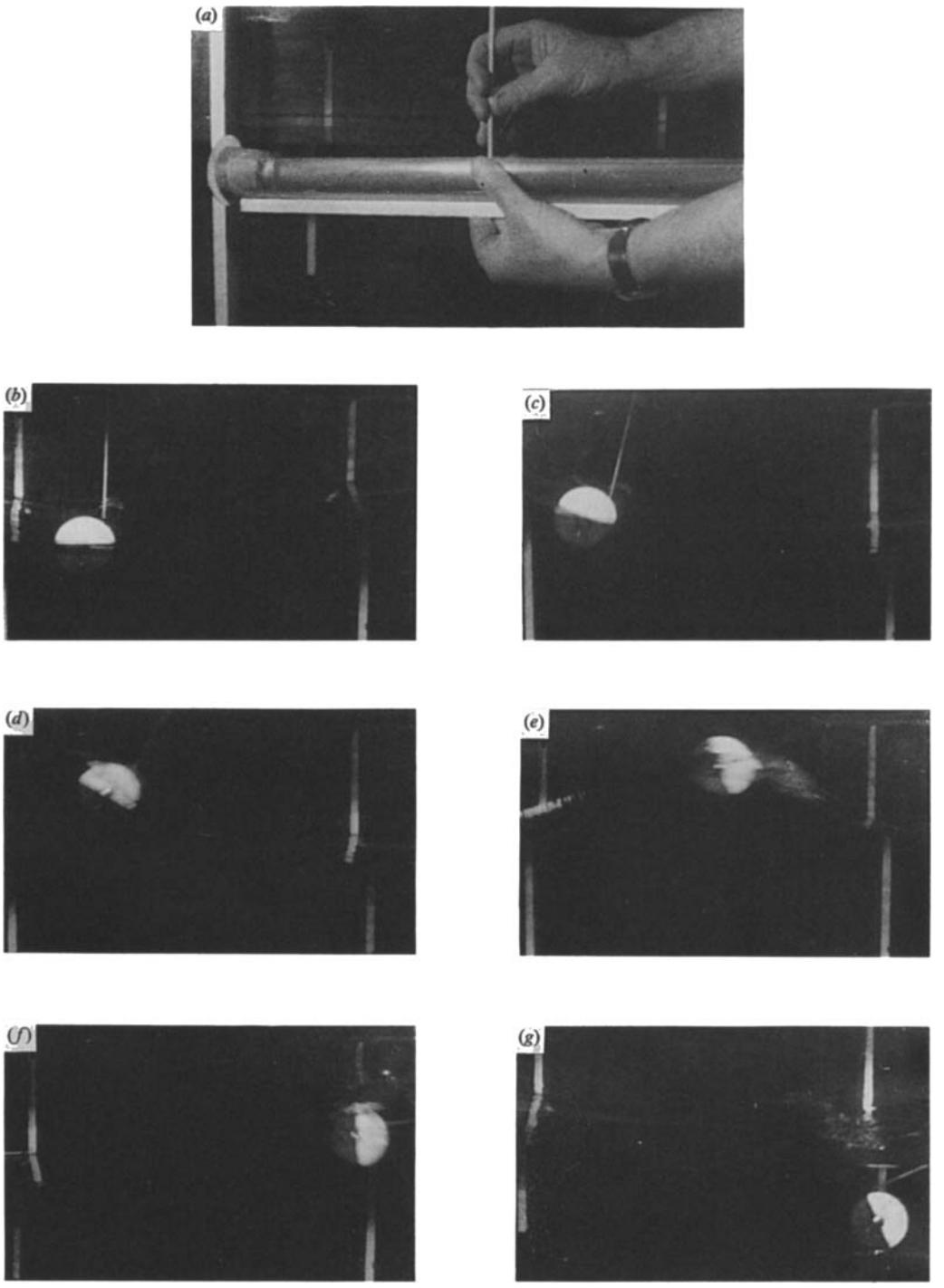

FIGURE 25. (*a*) Modified model hull, with keel and mast. (*b*)–(*g*) Model in very steep waves: $ak = 0.40$.

The conclusion is somewhat modified by considering the flow in an *almost-highest* wave, given by (4.5). On substituting for z in the general formula (7.1) we find

$$t = \int_0^{\phi} \frac{(\delta - \eta\psi)^2 + (\eta\phi)^2}{[(\beta+\psi)^2 + \phi^2]^{\frac{4}{3}}} \, \mathrm{d}\phi, \tag{7.13}$$

where

$$\delta = \tfrac{1}{3}\alpha - \beta\gamma, \quad \eta = \tfrac{2}{3}\gamma. \tag{7.14}$$

The corresponding lines of constant t are shown in figure 23. It will be seen that near the crest the loci of constant t are no longer tangential to the free surface, but they tend to become so as r/l becomes large. The approximation remains valid only so long as r/l is not large compared with $1/\epsilon$ (see Longuet-Higgins & Fox 1978).

8. Model experiments

A hollow Perspex tube, of length 50 cm, diameter 5 cm and wall thickness 3 mm, was bunged at both ends and fitted with a thin aluminium keel of width 12 mm, running the length of the cylinder (see figure 24*a*). To one end was attached a black-and-white cardboard disk to indicate the angle of roll. When floating in still water the cylinder was half submerged, with a free-roll period of 0.5 s.

The model was placed across the same channel, 60 cm wide, as described in §2, and subjected to wavetrains of period about 1.0 s, generated in the same manner. In low waves of steepness $ak = 0.07$ (figure 24*b*) the model tended to roll with the local wave surface, as in figure 21(*a*). In steeper waves, $ak = 0.23$, the phase of the roll was reversed (figure 24*c*). On passage of a very steep wave, $ak = 0.39$, the model was rolled through an angle of 60° or more (figure 24*d*).

A similar experiment with the same model, but without the keel, showed only a slight angle of roll.

To simulate an open boat, a similar cylindrical model was prepared, but with one-third of the circumference removed, the lost mass being made up by a wooden shaft fixed to the axis. To this was attached a very light balsa-wood mast (figure 25*a*). On placing the model in a steep wave it behaved similarly to the circular cylinder. Figures 25(*b–g*) show the boat rolling through nearly 90°, becoming swamped, and sinking to the bottom.

In the above experiments the waves were not breaking. Breaking waves did indeed produce even stronger rolling motions, as has been found in other capsizing studies (see for example Kirkman, Nagle & Salsich 1983). The significance of the present experiments is that catastrophic rolling may be induced even by non-breaking waves. Attention is also drawn to the probable part played in capsizing by an efficient keel.

The author is indebted to Dr Charles Clayson for constructing the accelerometer described in §5, and for assistance with the experiments. For an introduction to the literature on ship rolling and for useful comments, the author thanks Nick Newman.

REFERENCES

Ewing, J. A., Longuet-Higgins, M. S. & Srokosz, M. A. 1986 Measurements of the vertical acceleration in wind waves. *J. Phys. Oceanogr.* (in press).

Himeno, Y. 1981 Prediction of ship roll damping – state of the art. *University of Michigan, Dept of Naval Architecture Rep. No.* 239, *Sept.* 1981, 65 pp.

KIRKMAN, K. L., NAGLE, T. J. & SALSICH, J. O. 1983 Sailing yacht capsizing. *Proc. Chesapeake Sailing Yacht Symp., Annapolis Md. Jan. 1983*. New York: Soc. Nav. Arch. Mar. Eng.

LAMB, H. 1932 *Hydrodynamics*, 6th edn. Cambridge University Press, 738 pp.

LONGUET-HIGGINS, M. S. 1953 Mass transport in water waves. *Phil. Trans. R. Soc. Lond.* A **245**, 535–581.

LONGUET-HIGGINS, M. S. 1963 The generation of capillary waves by steep gravity waves. *J. Fluid Mech.* **16**, 138–159.

LONGUET-HIGGINS, M. S. 1974 Breaking waves – in deep or shallow water. *Proc. 10th Symp. on Naval Hydrodynamics, Cambridge, Mass. June 1974*, pp. 597–608. Arlington, Va., Office of Nav. Res., 792 pp.

LONGUET-HIGGINS, M. S. 1975 Integral properties of periodic gravity waves of finite amplitude. *Proc. R. Soc. Lond.* A **342**, 157–174.

LONGUET-HIGGINS, M. S. 1979*a* Why is a water wave like a grandfather clock? *Phys. Fluids* **22**, 1828–1829.

LONGUET-HIGGINS, M. S. 1979*b* The trajectories of particles in steep, symmetric gravity waves. *J. Fluid Mech.* **94**, 497–517.

LONGUET-HIGGINS, M. S. 1979*c* The almost-highest wave: a simple approximation. *J. Fluid Mech.* **94**, 269–273.

LONGUET-HIGGINS, M. S. 1985 Accelerations in steep gravity waves. *J. Phys. Oceanogr.* **15**, 1570–1579.

LONGUET-HIGGINS, M. S. 1986 The propagation of short surface waves on longer gravity waves. *Proc. R. Soc. Lond.* A. (in press).

LONGUET-HIGGINS, M. S. & FOX, M. J. H. 1977 Theory of the almost-highest wave: the inner solution. *J. Fluid Mech.* **80**, 721–740.

LONGUET-HIGGINS, M. S. & FOX, M. J. H. 1978 Theory of the almost-highest wave. Part 2. Matching and analytic extension. *J. Fluid Mech.* **85**, 769–786.

OCHI, M. K. & TSAI, C.-H. 1983 Prediction of breaking waves in deep water. *J. Phys. Oceanogr.* **13**, 2008–2019.

PHILLIPS, O. M. 1958 The equilibrium range in the spectrum of wind generated waves. *J. Fluid Mech.* **4**, 426–434.

SROKOSZ, M. A. 1986 A note on the probability of wave breaking. *J. Phys. Oceanogr.* **16**, 382–385.

SROKOSZ, M. A. & LONGUET-HIGGINS, M. S. 1986 On the skewness of sea-surface elevation. *J. Fluid Mech.* **164**, 487–497.

TAYLOR, G. I. 1921 Diffusion by continuous movements. *Proc. Lond. Math. Soc.* (ser. 2) **20**, 196–212.

TAYLOR, G. I. 1953 An experimental study of standing waves. *Proc. R. Soc. Lond.* A **218**, 44–59.

WILLIAMS, J. M. 1985 Near-limiting waves in water of finite depth. *Phil. Trans. R. Soc. Lond.* A **314**, 353–377.